Journal of Molecular Structure 1217 (2020) 128395

Contents lists available at ScienceDirect

Journal of Molecular Structure

journal homepage: http://www.elsevier.com/locate/molstruc

Synthesis of new fluorene compounds for highly selective sensing of picric acid, Fe^{3+} and L-arginine

Yingying Han , Jinxin Zhao , Haicheng Yang , Xintong Huang , Xinyue Zhou , Tianqi Hui , Jie Yan *

College of Chemistry and Chemical Engineering, Liaoning Normal University, Huanghe Road 850#, Dalian, 116029, PR China

ARTICLE INFO

Article history:
Received 5 December 2019
Received in revised form
18 March 2020
Accepted 5 May 2020
Available online 10 May 2020

Keywords:
Fluorene compounds
Synthesis
Fluorescence sensor
L-argnine

ABSTRACT

Two compounds, 4-(4-(7-bromo-9, 9-dimethyl-fluoren-2-yl) phenyl) pyridine (**4**) and 2, 7-Bis-(4-tert-butyl-phenyl)-9,9-dimethyl-9H-fluorene (**5**), were synthesized by bromination, methylation and Suzuki coupling reaction with fluorene as the starting material. The compounds were used as fluorescent sensors to detect some nitro compounds (NACs), metal cations and amino acids. The test results showed that the 4-(4-(7-bromo-9, 9-dimethyl-fluoren-2-yl) phenyl) pyridine (**4**) as fluorescence sensor **1** detected 2, 4, 6-Trinitrophenol (TNP) at the magnitude of 10 μM, with a sensitivity of K_{sv} was $4.6 \times 10^5\ M^{-1}$ and the detection limit was 6.9×10^{-7} M. The sensitivity detection for Fe^{3+} with K_{sv} value was $1.4 \times 10^5\ M^{-1}$, and the detection limit was 3.6×10^{-7} M. At the same time, it was found that 2, 7-Bis-(4-tert-butyl-phenyl)-9,9-dimethyl-9H-fluorene (**5**) as fluorescence sensor **2** also showed excellent selective recognition ability toward the arginine (L-arg) in biomolecules with K_{sv} values of $3.9 \times 10^4\ M^{-1}$, and the detection limit was 1.15×10^{-6} M for arginine (L-arg).

1. Introduction

As a new type of luminescent material in recent years, fluorescent organic compounds have been used as fluorescent probes to detect various organic substances, such as nitro aromatic explosives, anions, cations, and biological molecules [1,2]. Because of the sensitivity, selectivity, portability, short response time and convenience of visual detection, fluorescence detection has important potential applications in analysis, biology and clinical biochemistry [3–5]. Because fluorene polymers have many advantages, such as easy purification, clear structural characteristics and excellent hole transport capacity, and is a promising photoelectric material [6,7]. Therefore, more and more attention has been paid to the development and study of the fluorescent properties of fluorene compounds [8,9]. Nitro aromatic compounds are common components in explosives and are therefore widely used in industrial development [10]. Most nitro aromatic compounds are classified as dangerous drugs. Among them, 2, 4, 6-trinitrophenol (TNP) is considered as an extremely dangerous chemical due to its strong explosive capacity and low safety factor [11]. Some advanced equipment technology, such as gas chromatography, mass spectrometry, surface enhanced Raman spectroscopy, cyclic voltammetry and energy dispersive X-ray diffraction, neutron activation analysis and nuclear quadruple resonance are also available, but the required equipment is not easy to transport and operate, as a result, these technologies are not suitable for real-time detection [12–16]. The advantages of fluorescence detection for nitro compounds are portability and ease of use. Metal cations (such as Cr^{3+}, Fe^{3+} and Al^{3+}) play an important role in the environment and human health [17], among which iron is the most abundant metal element in cells and is widely found in many biological enzymes and proteins. The imbalance of Fe^{3+} involved in the metabolism of human cells can cause kidney failure, anemia and other diseases [18,19]. Because traditional detection methods usually have shortcomings such as low sensitivity, long analysis time and complicated operation [20]. It is necessary to develop fluorescent sensors that can detect Fe^{3+}. Amino acids are the building blocks of proteins, and they have a very important relationship with the life activities of organism [21]. Different kinds of amino acids have their own functions in organisms. Arginine (Arg) is particularly abundant in protamine and histones, and a lack of Arg can lead to a recessive genetic disorder called the urea cycle disorder [22–25]. Therefore, Arg has received extensive attention in the fields of biochemistry and medicine. At present, researchers generally synthesize different kinds of amino

* Corresponding author.
E-mail address: yhc1994@live.cn (J. Yan).

https://doi.org/10.1016/j.molstruc.2020.128395
0022-2860/

acid derivatives by reacting amino acid molecules with other compounds, thereby enhancing the sensitivity and selectivity of amino acids [26].

2. Experimental

2.1. Instruments and reagents

Infrared spectra were obtained on a Bruker AXS TENSOR-27 FT-IR spectrophotometer with pressed KBr tablet in the range of 4000−400 cm^{-1}. A JASCO-V-570UV/VIS/VIS/NIR spectrophotometer was used to record UV−vis absorption. Also, F-7000 fluorescence spectrometer (Hitachi, Japan) was used to record fluorescence emission studies. The mixed solvent V_{C2H5OH}/V_{H2O} (3:1) was selected as the solvent and a 1×10^{-5} M solution of the sensor **1** and sensor **2**. We take 3 mL and put them in quartz cuvette. A Bruker AV 500 OFT-NMR spectrometer can record ^1H NMR and ^{13}C NMR in $CDCl_3$-d_6 at 500 and 125 MHz respectively.

Dichloromethane, trichloromethane, absolute ethyl ethanol, dimethyl sulfoxide, dioxane, petroleum ether and ethyl acetate were all analytically pure. Terakis(triphenylphosphine)palladium was purchased from Shanghai Sinopharm Company, and other chemicals and reagents were purchased from Tianjin Komiou Chemical Reagent Co., Ltd.

2.2. Synthesis of 2, 7-dibromo-9H-fluorene (2)

Fluorene (10.0 g, 60 mmol) in 150 mL chloroform was added into a 250 mL three-necked flask and was stirred at room temperature to dissolve all fluorene. After being dissolved for 0.5 h, anhydrous ferric chloride (150 mg, 0.92 mmol) was added to the system, and the whole reaction system was wrapped in tin foil. The whole reaction system was then cooled to 0 °C in an ice water bath after stirring and avoiding light. The constant pressure drop funnel was used to slowly add bromine (6.4 mL, 123 mmol) into the system. When the drop was completed for 1.5−2 h, the ice water bath was removed, and the temperature of the system was slowly raised to room temperature continuing 3 h. After the reaction, 200 mL saturated sodium thiosulfate solution was gradually added into the system with stirring, and the red color of the system completely disappeared. The bottom layer was extracted with dichloromethane for 3−4 times, and the organic phase was combined. The organic phase was dried with anhydrous magnesium sulfate, and the rotary evaporation was used to remove dichloromethane to obtain a pale yellow solid. The solid was added with 120 mL anhydrous ethanol and refluxed to be dissolved completely. After cooling and filtering, the crude product was recrystallized in ethanol to obtain 17.24 g white needle-like crystal with the yield of 88.4%.

2, 7-Dibromo-9H-fluorene **(2)**: IR (KBr), ν/cm^{-1}: 3056 (=CH— stretching); 2924, 2855 (C−H stretching); 1598, 1575, 1455 (Ph skeleton vibration); 1397 (C−H bending).

^1H NMR (500 MHz, $CDCl_3$, δ/ppm): 7.61 (s, 2H, Flu-H^1 and Flu-$H^{1'}$), 7.54−7.52 (d, $J = 8.1$ Hz, 2H, Flu-H^3 and Flu-$H^{3'}$), 7.47−7.45 (dd, $J_1 = 8.1$ Hz, $J_2 = 1.5$ Hz, 2H, Flu-H^2 and Flu-$H^{2'}$), 3.79 (s, 2H, CH_2).

2.3. Synthesis of 2, 7-dibromo-9, 9-dimethyl-fluorene (3)

2, 7-Dibromo-9H-fluorene (13.2 g, 40 mmol) was poured into a 250 mL three-necked flask. Then measuring 70 mL dimethyl sulfoxide and adding it to the three-necked flask. Stirring at room temperature until the solid is completely dissolved. Potassium hydroxide (10.0 g, 179 mmol) was crushed in a mortar and added to a three-necked flask to turn the solution into purple black. Continuing to stirring and heating the oil bath to 35 °C.The mixture of methyl iodide (12.5 g, 88 mmol) and dimethyl sulfoxide (80 mL) was added by the constant pressure drop funnel for 8 h, and then the reaction was continued for 12 h. Finally, the reaction was cooled to room temperature. The reaction solution was poured into a beaker containing 250 mL water, and the purple solid was precipitated, then filtered and dried. The solid was added to 80−100 mL anhydrous ethanol and reflux dissolves it completely. Then the crude product was filtered and recrystallized by the ethanol to obtain 12.38 g yellow needle-like crystal with the yield of 86.3%.

2, 7-Dibromo-9, 9-dimethyl-fluorene: IR (KBr), ν/cm^{-1}: 3028 (=CH— stretching); 2966, 2923, 2866, (C−H stretching); 1595, 1576, 1447 (Ph skeleton vibration); 1397 (C−H bending).

1H NMR (500 MHz, $CDCl_3$, δ/ppm): 7.53−7.51 (m, 4H, Flu-H1, Flu-H1', Flu-H3 and Flu-H3'), 7.45−7.43 (dd, J1 = 8.1 Hz, J2 = 1.2 Hz, 2 H, Flu-H2 and Flu-H2'), 1.45 (s, 6 H, CH3).

2.4. Synthesis of 4-(4-(7-bromo-9, 9-dimethyl-fluoren-2-yl) phenyl) pyridine (4)

9, 9-dimethyl-2, 7-dibromofluorene (5.6 g, 16 mmol) and potassium phosphate (5.1 g, 96 mmol) were added to a three-necked flask which containing 100 mL dioxane, and terakis(-triphenylphosphine)palladium (1.1 g, 0.45 mmol) were added for nitrogen protection. In addition, 4-(4-pyridinyl)phenoboric acid (5.73 g, 32 mmol) was dissolved with 80 mL dioxane in constant pressure drop funnel and added it into three-necked flask drop by drop. Then the system was heated up to 85 °C, and slowly heated up to 110 °C with refluxing for 24 h. Finally, the reaction solution was extracted with ethyl acetate and saturated salt water before being dried over $MgSO_4$. After drying under reduced pressure, the intermediate product was purified by silica gel column chromatography using petroleum ether and ethyl acetate with a volume ratio of 1:2. The pale yellow flake crystal was obtained with a yield of 56%.

4-(4-(7-bromo-9,9-dimethyl-fluoren-2-yl) phenyl) pyridine (**4**): IR (KBr), ν/cm^{-1}: 3432 (O−H stretching); 3019 (=CH— stretching); 2927, 2849 (C−H stretching); 1598, 1454 (Ph skeleton vibration); 1398 (C−H bending); 1264 (C−N asymmetric stretching).

^1H NMR (500 MHz, $CDCl_3$, δ/ppm): 8.72 (s, 2H, Py-H^9, Py-$H^{9'}$), 7.81−7.75 (m, 5H, Py-H^8, Py-$H^{8'}$, Flu-H^4, Flu-$H^5$and Flu-H^6), 7.69 (s, 1 H, Flu-H^1)7.69−7.60 (m, 5H, Py-H^7, Py-$H^{7'}$and Flu-H^3), 7.51 (d, $J = 8.1$ Hz, 1 H, Flu-H^2))1.45 (s, 6 H, CH_3).

^{13}C NMR (125 MHz,$CDCl_3$,δ/ppm):157.4, 155.5, 151.2, 149.7, 143.8, 141.2, 139.4, 139.1, 138.1, 131.7, 129.3, 128.9, 127.8, 127.6, 122.8, 122.7, 121.9, 48.7, 28.5.

2.5. Synthesis of 2, 7-bis(4-(tert-butyl)phenyl)-9, 9-dimethyl-9h-fluorene (5)

Weighing 9, 9-dimethyl-2, 7-dibromofluoren (5.6 g, 16 mmol), potassium phosphate (5.1 g, 96 mmol), 4-tert-butylbenzeneboronic acid (5.73 g, 32 mmol), terakis(triphenylphosphine)palladium (1.1 g, 0.45 mmol), and 100 mL dioxane were added to a three-necked flask and protected with nitrogen. The system was refluxed at 110 °C for 24 h. After that, the reaction solution was extracted with ethyl acetate and brine for 3 to 4 times. The organic layer was dried over anhydrous magnesium sulfate, and then reduced pressure rotary evaporation left a small amount of solution. The mixed solvent was subjected to column chromatography using petroleum ether and dichloromethane with a volume ratio of 20:1 to obtain 5.46 g pale yellow needle crystals and the yield is 57.6%.

2, 7-bis(4-(tert-butyl)phenyl)-9, 9-dimethyl-9h-fluorene.(IR: (KBr), σ/cm^{-1}: 3451 (ν-OH), 3032 ((ν Ar−H), 2960、2875 (ν −CH_2-), 1625、1513、1461 (ν Ar), 1363 (δ-C-H).

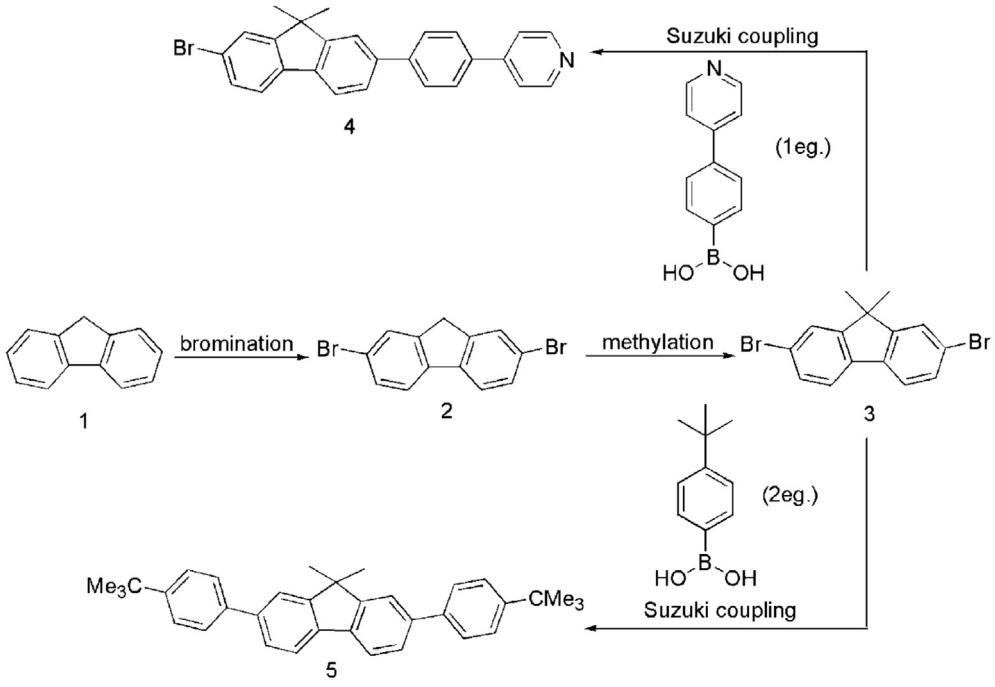

Scheme 1. Synthetic routes.

^{1}H NMR (500 MHz, $CDCl_3$, δ/ppm): 7.79 (d,J = 7.9Hz,2 H,Ph-$H^{3,3\prime}$), 7.66 (s,2 H,Ph-$H^{2,2\prime}$), 7.63 (d,J = 7.8Hz,2 H, Ph-$H^{4,4\prime}$), 7.59 (d,J = 7.8Hz,4 H, Ph-$H^{5,5\prime,6,6\prime}$), 7.51 (d,J = 7.7Hz,4H,Ph-$H^{7,7\prime,8,8\prime}$), 1.58 (s,6 H,$CH_3^{1,1\prime}$),1.39 (s,18 H,CH_3).

^{13}C NMR (125 MHz,$CDCl_3$,δ/ppm):153.9, 149.7, 139.7, 138.2, 137.4, 126.3, 125.6, 125.2, 120.8, 119.7, 46.5, 34.0, 30.9, 26.7.

The synthetic routes and detailed procedures are shown in Scheme 1. 2, 7-Dibromo-9H-fluorene (**2**) and 2, 7-Dibromo-9, 9-dimethyl-fluorene (**3**) were synthesized by methods reported in the literature [27,28]. The synthesis of the compound **2** is improved by the original literature method, by adding KOH first, followed by mixing with 2, 7-Dibromo-9H-fluorene, and then adding a mixture of methyl iodide and the solvent of DMSO. This can make 2, 7-Dibromo-9H-fluorene fully form carbon anions under alkaline action, which is more favorable for nucleophilic substitution reaction with CH_3I. In addition, when using anhydrous ethanol for recrystallization, the solvent was firstly stirred at room temperature for 4 h and then refluxed by heating. Which raised the yield to 86.3% (literature yield: 76%). Two rare new multifunctional fluorescent fluorene derivatives were synthesized by Suzuki coupling reaction: 4-[4-(7-bromo-9,9-dimethyl-9H-fluoren-2-yl)phenyl]pyridine (**4**) and 2, 7-bis (4-(tert-butyl)phenyl)-9, 9-dimethyl-9h-fluorene (**5**). In conclusion, the systematic synthesis of new fluorene materials and the efficient detection of TNP, ferric ion and amino acid are the focus of this paper.

Compounds **2**, **3** and **4** were confirmed by single crystal structure. Fig. 1 shows the structure unit diagram of compound **4**. X-ray single crystal study shows that compound **4** CCDC (1,581,412) is crystallized in a monoclinic system with P2 (1) 1/c space group. The crystallographic data of compounds **2**, **3** and **4** (Figure S1A) and main bond length (Figure S1B) were also obtained.

3. Result and discussion

3.1. Emission spectra study of compounds

The emission spectra of fluorene and compounds **2**, **3**, **4** and **5**, as shown in Fig. 2, were measured at a voltage of 500 V, a slit width of 5:5, and an excitation wavelength of 280 nm. For compounds **2** and **3**, we can see that almost no fluorescence intensity is detected. The maximum emission wavelength of fluorene was measured by 313 nm, and for compound **4**, the maximum emission wavelength

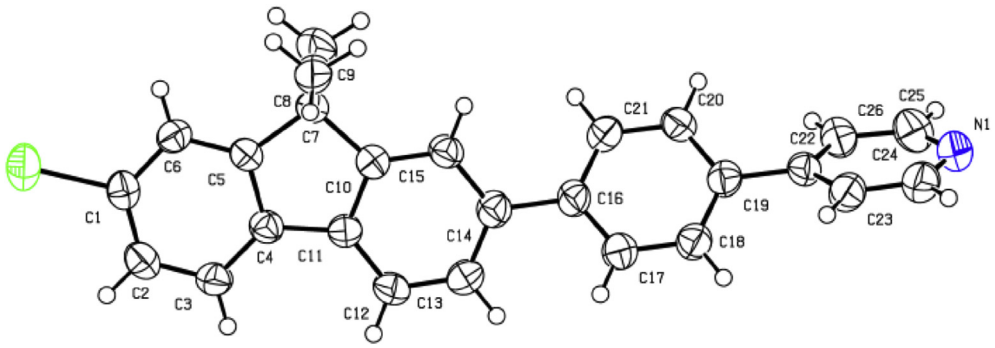

Fig. 1. The crystal structure of compound **4** (hydrogen atoms are omitted for clarity).

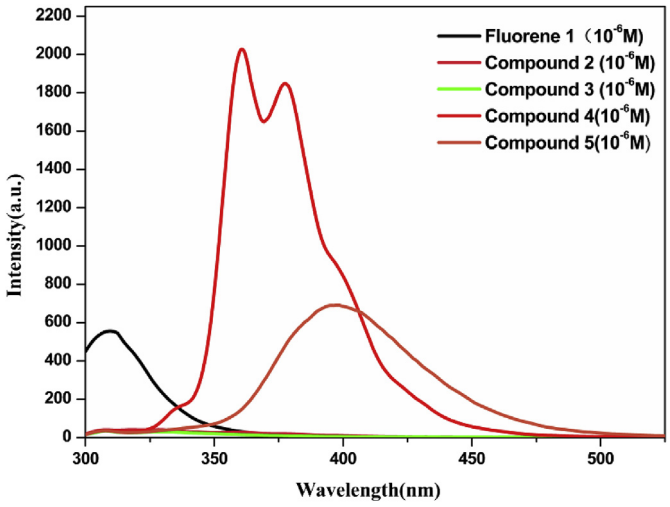

Fig. 2. The fluorescence spectra of fluorene **1** and compounds **2**、**3**、**4**、**5** in C_2H_5OH.

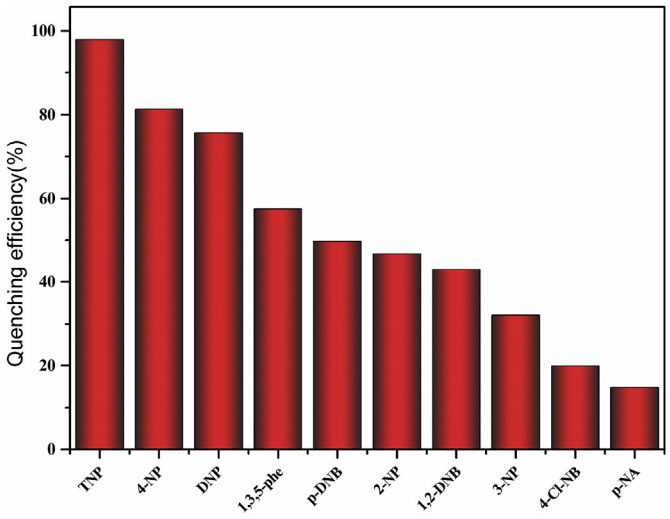

Fig. 3. The column graph of sensor **1** reduction in fluorescence intensity (plotted as quenching efficiency) upon the addition of different analytes.

was 400 nm, and the compound **5** was 367 nm. Compared with fluorene, compound **1** and compound **3** exhibited significant fluorescence quenching, and the maximum emission wavelength of compound **4** appeared red-shifted. Compounds **2** and **3** are containing bromine atoms. Under the condition of containing a halogen atom, the excited state of the compound and the heavy atom forms a composite material in a ratio of 1:1, and the degree of spin orbital coupling in the composite is much greater than that of the normal compound, and fluorescence quenching occurs [29,30]. Although compound **4** also contains a bromine atom, compound **4** has a benzene ring and a pyridine, which increases the conjugated chain, resulting in a significant red-shift during fluorescence detection. The benzene and the tert-butyl group are added to the compound **5**, and the maximum emission wavelength is blue-shifted compared with the compound **4**. It is presumed that the presence of the tert-butyl group causes the molecular skeleton of the original conjugated system to be distorted, and the conjugation effect was weakened.

3.2. Fluorescence detection of partial nitro compounds

When the mixed solvent V_{C2H5OH}: V_{H2O} = 3:1 was selected as the solvent and different nitro aromatic compounds were added to the sensor with 10^{-5} M^{-1} concentration under the excitation wavelength of 320 nm, the fluorescence intensity was significantly decreased. We selected TNP (2,4,6-trinitrophenol), 4-NP (4-nitrophenol), DNP (2,4-dinitrophenol), 1,3,5-phe (phloroglucin), p-DNB (p-dinitrobenzene), 2-NP (2-nitrophenol), 1,2-DNB (o-dinitrobenzene), 3-NP (3-nitrophenol), 4-Cl-NB (4-chloronitrobenzene), p-NA (p-nitroacetophenone). As shown in Fig. 3, by calculating the quenching percentage of several analytes ($Q_P=(I_0-I)/I_0 \times 100\%$, I_0 and I are the luminescence intensity before and after the addition of the nitro compound to the sensor). The quenching percentage of sensor **1** for several analytes was as follows:97.86%, 81.25%,75.61%, 57.44%, 49.73%,46.75%, 42.95%, 32.03%, 19.83%, and 14.81%. The order of quenching efficiency is TNP>4-NP > DNP>1,3,5-phe > p-DNB>2-NP>1,2-DNB>3-NP>4-Cl-NB > p-NA. The quenching efficiency revealed that TNP has faster fluorescence quenching over the other nitro aromatic compounds. We need to calculate the Stern-Volmer constants of the quenching process.

We evaluated the sensitivity by the Stern-Volmer equation (1) [31],

$$I_O / I = K_{SV} [Q] + 1 \quad (1)$$

Where K_{SV} represents the Stern-Volmer constant and is used to indicate the sensitivity of the sensor. A liner relationship for Stern-Volmer plot was obtained for TNP with correlation coefficient (R^2) equal to 0.97 as shown in Fig. 4(B). I_0 and I represent the fluorescence intensity before and after the analyte is added, [Q] is the molar concentration of the analyte. As shown in Fig. 4(A), the K_{SV} curve began to curve upward as the concentration of the analyte increased. As shown in Fig. 4(C), it can be seen more intuitively that the linear relationship exhibited at lower concentrations is mainly due to static quenching, while the linear deviation at higher concentrations may be due to dynamic quenching. Static quenching is usually due to the interaction of the ground state between the analyte and the sensor. Dynamic quenching is mainly attributed to energy and electron transfer between analyte and sensor. Fitting of liner parts allows the quenching constants of sensor **1** to be 8910 M^{-1} for 2-NP, 7555 M^{-1} for 1, 2-DNB, 464546 M^{-1} for TNP, 9677 M^{-1} for p-DNB, 2328 $M^{-1}$for 4-cl-NB, 29903 M^{-1} for DNP, 13535 M^{-1} for 1,3,5-phe, 1696 M^{-1} for p-NA, 43912 M^{-1} for 4-NP, 4691 M^{-1} for 3-NP. In addition, the sensor's detection limit (LOD) for TNP is calculated by equation (2) [32],

$$LOD = 3\,\sigma/k \quad (2)$$

Where σ is the standard deviation of the measured blank and k is the slope between the fluorescence intensity and the TNP concentration. After calculation, sensor **1** has a detection limit of 0.69 μM for TNP. Present sensor **1** for TNP detection is considerably below the values of detection limits recently reported methods in Table 1.

3.2.1. Fluorescence detection of cations

The compound 2,7-bis(4-(tert-butyl)phenyl)-9,9-dimethyl-9H-fluorene was used as a sensor which emitted blue fluorescence with a maximum excitation wavelength of 320 nm. Under the same conditions, we added Fe^{3+}, Pb^{2+}, Al^{3+}, Mg^{2+}, Fe^{2+}, Cr^{3+}, Mn^{2+}, Ni^{2+}, Zn^{2+}, Cu^{2+}, Co^{2+} and Cd^{2+} ions to the sensor with a concentration of 10^{-5} M to detect the fluorescence intensity of the sensor. As shown in Fig. 5, it can be seen that Fe^{3+} has the best quenching effect on the sensor under the same concentration conditions. The experimental results showed that the sensor has higher selectivity

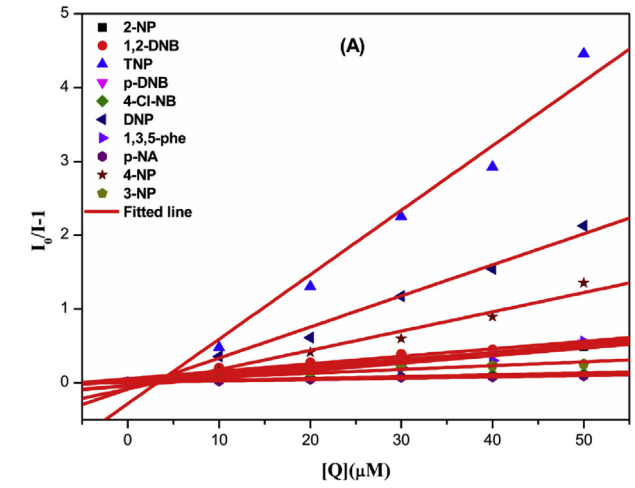

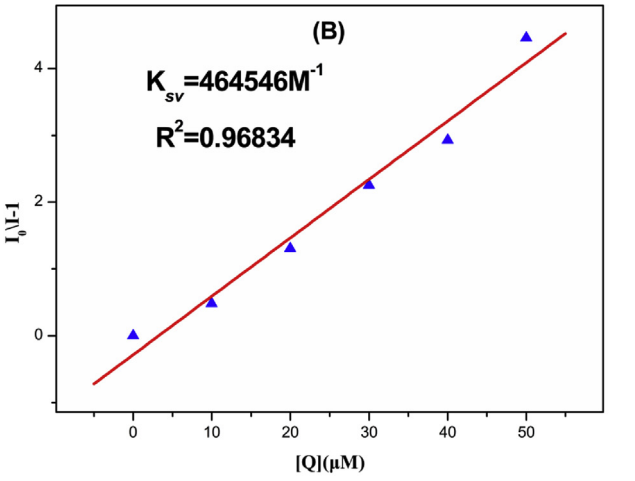

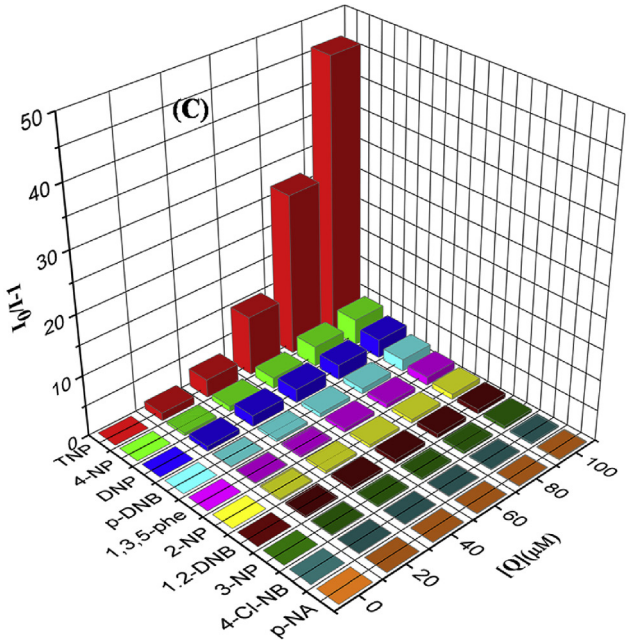

Table 1
Comparative study of present sensor with previously reported sensors.

Material	LOD.(μM)	Solvent Condition
Heterocyclic aromatic chlorides	0.78([33])	Aqueous DMSO
Hydrazide Schiff	0.99([34])	Pure Aquatic
Antipyrine Derivatives	1.74([35])	H2O:THF(7:3)
Tris-Imidazolium Derivatives	2.04([36])	DMSO
Flourene Derivatives	0.69(present work)	C2H5OH:H2O(3:1)

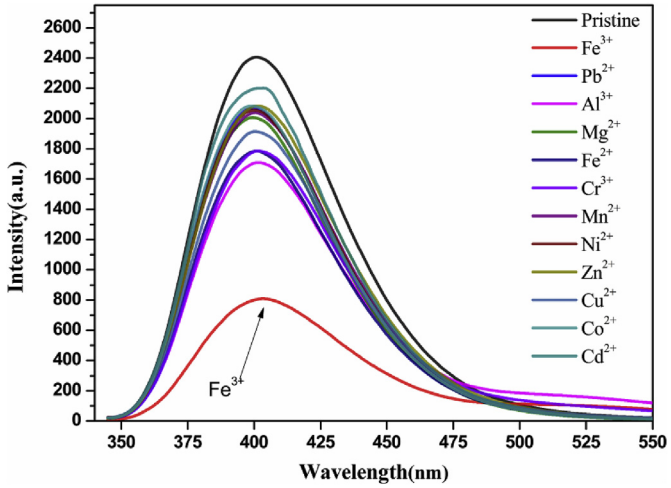

Fig. 5. The fluorescent response of sensor **1** (10 μM) to selected metal ions (100 μM).

to Fe^{3+}.

3.2.2. Micro-detection of ferric ions

In order to further investigate the effect of Fe^{3+} concentration on the fluorescence intensity of sensor **1**, increase the Fe^{3+} concentration to 200 μM, and the fluorescence spectrum is shown in Fig. 6. As the concentration of Fe^{3+} is increased, the luminous intensity of the sensor **1** decreased remarkably. When the concentration is increased to 160 μM, the peak value reaches a minimum value. The peak intensity reached the minimum with the 3.1-fold (I_0/I) decreasing when 160 μM equiv of Fe^{3+} ions were added in. When the concentration of Fe^{3+} was increased from 160 to 200 μM, the fluorescence intensity of the sensor did not change significantly. The sensitivity constant of sensor **1** for Fe^{3+} is 142098.8 M^{-1}, and the detection limit for Fe^{3+} is 0.36 μM by formula $I_0/I = K_{SV}[Q] + 1$ and formula detection limit = 3σ/k.

3.3. Detection of biological small molecules

4-(4-(7-bromo-9, 9-dimethyl-fluoren-2-yl) phenyl) pyridine (**4**) as sensor **2** emitted light green fluorescence with a maximum excitation wavelength of 367 nm. The sensor **2** was used as a fluorescent probe to investigate the effect of different kinds of amino acids on the fluorescence intensity. Eight common amino acids were selected: L-methylthiol (L-met), DL-valine (DL-val), D-phenylalanine (D-phe), (L-arg) L-leucine (L-leu), L-glutamic acid (L-glu), L-aspartic acid (L-asp), glycine (gly). We added eight different amino acids (50 equivalents) to a 10^{-5} M sensor and examined their

Fig. 4. (A) Plot of I_0/I of sensor **1** (λ_{ex} = 325 nm and λ_{em} = 400 nm) versusconcentration of analytes in lower concentration ranges of analytes (up to 50 μM). (B) Stern–Volmer plots in different concentration ranges of TNP of sensor **1**(up to 50 μM). (C) The 3D bars of reduction in fluorescene intensity of analytes in concentration range of analytes for sensor **1** (up to 100 μM).

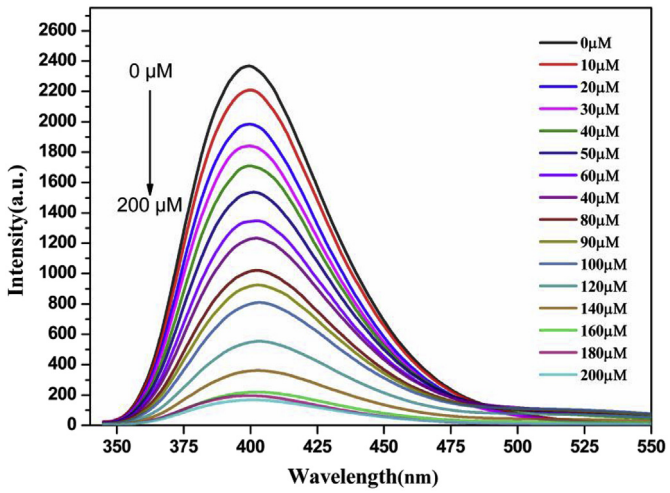

Fig. 6. Fluorescence quenching spectra of sensor **1** (10 μM) with different concentration of Fe^{3+} (0–200 μM).

effect on the luminescence intensity behavior of the sensor. The results are shown in Fig. 7 (A). As can be seen from the figure, the sample showed higher selectivity for L-arginine. The fluorescence intensity of other amino acids did not change much. In order to further explore the quenching response of L-arginine to the sensor, we changed the concentration of L-arginine added. The experimental results are shown in Fig. 7 (B). From the experimental results, it can be seen that with the increase of L-arginine concentration, the fluorescence intensity decreased gradually, and the cause of fluorescence quenching may be related to the change of free energy. When the sensor donor interacts with Arg, the electron transfer is from the large π bond to −C═N-. Therefore, when the concentration of L-arginine is continuously increased, the fluorescence intensity is gradually decreased. Moreover to understand the extent and nature of fluorescence quenching in sensor **2** by L-arg, plotting the normalized fluorescence intensity at 367 nm as a function of [L-arg] resulted in a nice liner relationship. A linear relationship for L-arg with correlation coefficient (R^2) equal to 0.99. The sensitivity constant of sensor **2** to L-arg is $3.9 \times 10^4\ M^{-1}$ by the formula $I_0/I = K_{SV}[Q] + 1$ and the formula of detection limit = 3σ/k, and the detection limit for L-arg is 1.15 μM.

3.4. Fluorescence quenching mechanism

To better understand sensors **1** have better quenching effects. We explain this by using an electronic donor-receptor system between the sensor and TNP. Since TNP is an electron-deficient molecule, when the electron-deficient LUMO is located between the HOMO and LUMO of electron-fluorene molecules, the mutual conversion between electrons can cause sensing during excitation. In the excitation process, the charge is transferred from the LUMO of the sensor to the LUMO of TNP, resulting in fluorescence quenching.

The HOMO and LUMO energies of the sensor and TNP are calculated by density functional theory (DFT), as shown in Fig. 8, showing that the LUMO of electron-deficient TNP is located between the HOMO and LUMO of the sensor. The energy difference between LUMO and TNP indicates that TNP has a good fluorescence quenching ability.

In addition, to demonstrate the charge transfer mechanism between the sensor and TNP, we performed a series of calculations using the DFT. In the presence of TNP, the geometric optimization of the sensor proves the most favorable position (in terms of energy) for the interaction between TNP and the sensor. If TNP and the sensor form a charge transfer complex, the LUMO energy of the newly formed complex should be lower than that of the sensor itself, while the HOMO energy is almost unchanged.

As shown in Fig. 8, the energy diagrams of sensor **1**, [sensor **1** + TNP] and TNP show that in the presence of TNP, the initial HOMO and LUMO energy difference of sensor **1** falls from 4.13 to 2.55 eV. During this process, the LUMO energy (−1.61 eV) of sensor **2** decreased by 1.62 eV compared to the LUMO energy (−3.23 eV) of the complex [sensor **1** + TNP], while the HOMO energy did not change significantly.

4. Conclusions

This paper takes fluorene as the starting material. Two new

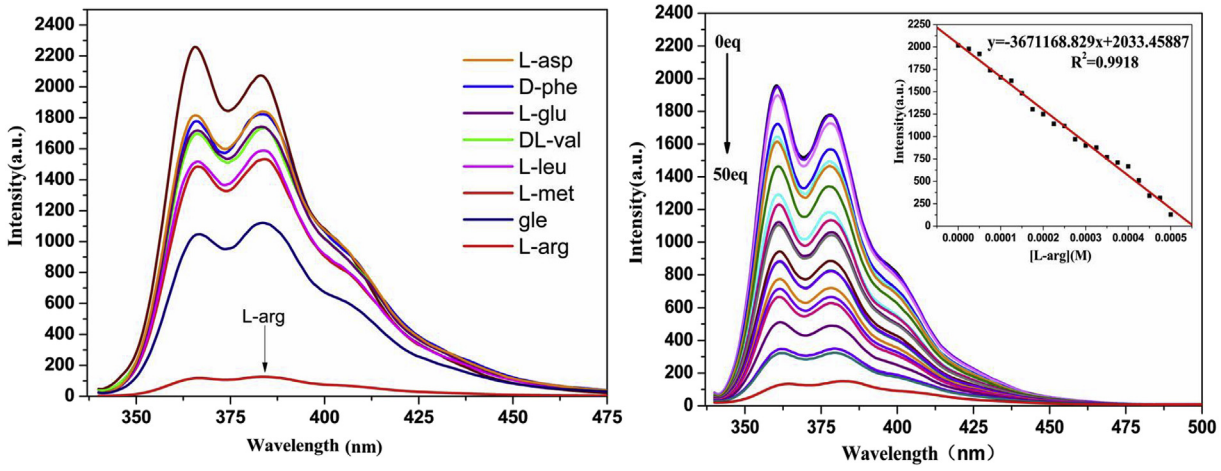

(A) (B)

Fig. 7. (A) The fluorescent response of sensor (10 μM) in the presence of different species amino acids (50 equiv.). (B) The fluorescence spectra of sensor (10 μM) in the presence of L-arg (050 equiv.). Inset shows the change in fluorescene intensity at 367 nm against various equiv. of L-arg (050 equiv.).

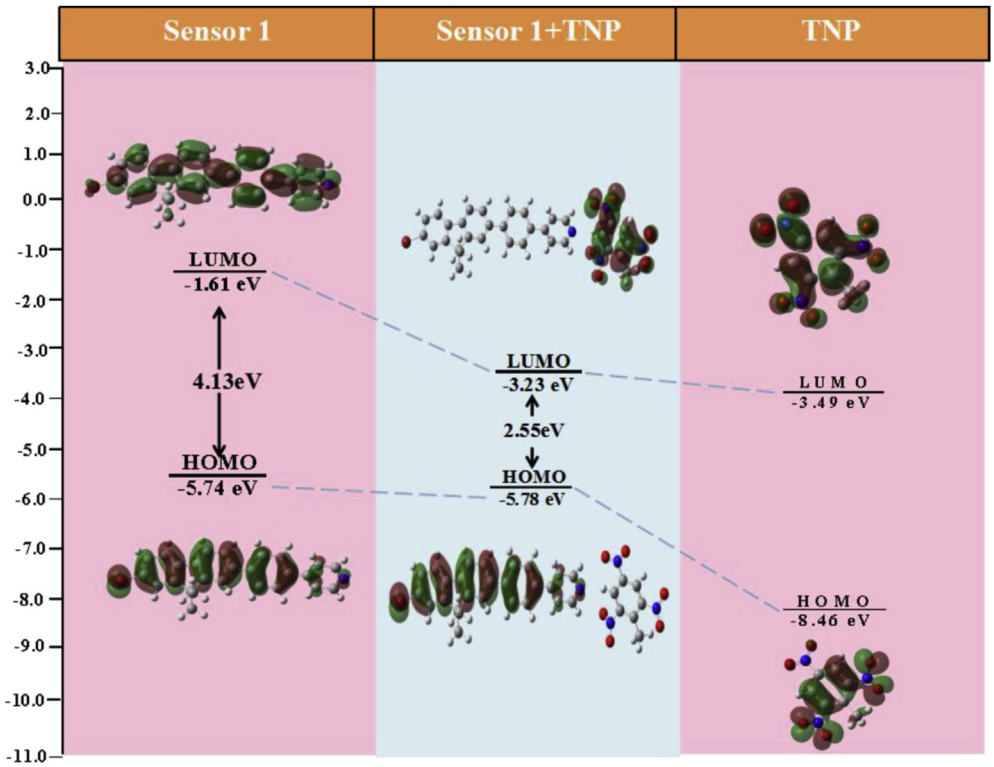

Fig. 8. Calculated energy level diagram of sensor **1**, TNP and [sensor **1** + TNP].

fluorene compounds, 4-(4-(7-bromo-9,9-dimethyl-9h-fluorene-2-) phenyl)pyridine(**4**) and 2,7-bis(4-(tert-butyl)phenyl)-9,9-dimethyl-9h-fluorene(**5**)were synthesized by bromine reaction, methylation reaction and Suzuki coupling reaction. The synthesized products were characterized by infrared spectroscopy, ^{1}H NMR, ^{13}C NMR and high resolution mass spectrometry. Some nitro aromatic compounds (NACs) and metal cation were detected by using 4-(4-(7-bromo-9,9-dimethyl-9h-fluorene-2-)phenyl)pyridine as fluorescence sensor **1**. The results showed that 4-(4-(7-bromo-9,9-dimethyl-9h-fluorene-2-) phenyl) pyridine had high detection sensitivity and low detection limit for TNP, ferric ion, and was a new bifunctional fluorescent detection compound. And 2,7-bis(4-(tert-butyl)phenyl)-9,9-dimethyl-9h-fluorene(**5**) also showed excellent selective recognition ability toward the arginine (L-arg) as fluorescence sensor **2** in biomolecules.

Declaration of competing interest

The authors declare that they have no known competing financial interests or personal relationships that could have appeared to influence the work reported in this paper.

CRediT authorship contribution statement

Yingying Han: Writing - original draft, Software. **Jinxin Zhao:** Writing - review & editing. **Haicheng Yang:** Writing - review & editing. **Xintong Huang:** Writing - review & editing. **Xinyue Zhou:** Conceptualization. **Tianqi Hui:** Conceptualization. **Jie Yan:** Writing - review & editing.

Acknowledgements

We are grateful for support provided by the Basic Natural Science Research, China Project of Liaoning Education Department(Grant No. LJ2019008).

Appendix A. Supplementary data

Supplementary data to this article can be found online at https://doi.org/10.1016/j.molstruc.2020.128395.

References

[1] G.Q. Lan, R.T. Dong, N.Q. Yu, L.M. Zhang, Y.Z. Ma, C.F. Yang, H. Deng, Construction of three new coordination polymers based on 5-ethyltetrazole (ET) generated via in situ cycloaddition reaction, Inorg. Chem. Commun. 24 (2012) 190–194, https://doi.org/10.1016/j.inoche.2012.07.007.
[2] X.D. Zhu, K. Zhang, W.X. Zhou, Q.H. Li, Y.Q. Fu, R.M. Liu, G.X.A. Qian, Luminescent two-fold interpenetrated pillared-layer metal-organic framework for highly selective and sensitive sensing of Fe^{3+}, Inorg. Chem. Commun. 73 (2016) 90–93, https://doi.org/10.1016/j.inoche.2016.10.009.
[3] V.K. Gupta, B. Sethi, R.A. Sharma, S. Agarwal, A. Bharti, Mercury selective potentiometric sensor based on low rim functionalized thiacalix [4]-arene as a cationic receptor, J. Mol. Liq. 177 (2013) 114–118, https://doi.org/10.1016/j.molliq.2012.10.008.
[4] V.K. Gupta, L.P. Singh, R. Singh, N. Upadhyay, S.P. Kaur, B. Sethi, A novel copper(II)selective sensor based on Dimethyl 4, 4′(o-phenylene)bis(3-thioallophanate) in PVC, matrix, J. Mol. Liq. 174 (2012) 11–16, https://doi.org/10.1016/j.molliq.2012.07.016.
[5] E.V. Antina, N.A. Bumagina, A.I. V'Yugin, A.V. Solomonov, Fluorescent indicators of metal ions based on dipyrromethene platform, Dyes Pigments 136 (2017) 368–381, https://doi.org/10.1016/j.dyepig.2016.08.070.
[6] Z.K. Peng, S.L. Tao, X.H. Zhang, G.X. Tang, X. Tao, C.S. Lee, S.T. Lee, New fluorene derivatives for blue electroluminescent devices: influence of substituents on thermal properties, photoluminescence, and electroluminescence, J. Phys. Chem. C 112 (6) (2008) 2165–2169, https://doi.org/10.1021/jp074834g.
[7] M.R. Zhu, T.L. Ye, C.G. Li, Efficient solution-processed nondoped deep-blue organic light-emitting diodes based on fluorene-bridged anthracene derivatives appended withCharge transport moieties, J. Phys. Chem. C 115 (36) (2011) 17965–17972, https://doi.org/10.1021/jp203892q.
[8] N. George, R. Subha, A.R. Thomas, N.L. Mary, Plasmon enhanced two-photon absorption in modified Styrene–Maleic Anhydride Silver nanocomposites, Nano-Structures & Nano-Objects 11 (2017) 32–38, https://doi.org/10.1016/j.nanoso.2017.05.011.
[9] K. Srinivasan, K. Subramanian, K. Murugan, G. Benelli, K. Dinakaran, Fluorescence quenching of MoS_2 nanosheets/DNA/silicon dot nanoassembly:

effective and rapid detection of Hg^{2+} ions in aqueous solution, Sci. Pol. R. 25 (11) (2018) 10567–10576, https://doi.org/10.1007/s11356-018-1472-x.
[10] D.K. Singha, P. Mahata, Optical detection of submicromolar levels of nitro explosives by a submicron sized metal–organic phosphor material, *J. Mater. Chem.* A. 2 (48) (2014) 20908–20915, https://doi.org/10.1039/c4ta05014b.
[11] D. Singha, M.P. Kanti, Detection of pesticides in aqueous medium and in fruit extracts using a three-dimensional metal–organic framework: experimental and computational study, RSC Adv. 5 (36) (2015) 28092–28097, https://doi.org/10.1021/acs.inorgchem.8b01767.
[12] Y. Ma, S. Wang, L. Wang, Highly selective and sensitive fluorescent paper sensor for nitroaromatic explosive detection, Trends Anal. Chem. 65 (2015) 13, https://doi.org/10.1021/ac302138c.
[13] K.K. Kartha, A. Sandeep, V.K. Praveen, A. Ajayaghosh, Detection of nitroaromatic explosives with fluorescent molecular assemblies and π-gels 3, Chem. Rec. 15 (2015) 252, https://doi.org/10.1002/tcr.201402063.
[14] F. Akhgari, H. Fattahi, Y.M. Oskoei, Recent advances in nanomaterial-based sensors for detection of trace nitroaromatic explosives, Sens. Actuators, B 221 (2015) 867, https://doi.org/10.1016/j.snb.2015.06.146.
[15] S. Shanmugaraju, P.S. Mukherjee, π-Electron rich small molecule sensors for the recognition of nitroaromatics, Chem. Commun. 51 (2015) 16014, https://doi.org/10.1039/C5CC07513K.
[16] S.J. Toal, W.C. Trogler, Polymer sensors for nitroaromatic explosives detection, J. Mater. Chem. 16 (2006) 2871, https://doi.org/10.1039/B517953J.
[17] R. Alam, R. Bhowmick, A.S.M. Islam, A. Katarkar, K. Chaudhurib, M. Ali, A rhodamine based fluorescent trivalent sensor (Fe^{3+}, Al^{3+}, Cr^{3+}) with potential applications for live cell imaging and combinational logic circuits and memory devices, New J. Chem. 41 (16) (2017) 8359–8369, https://doi.org/10.1039/C7NJ01675A.
[18] A.S. Pithadia, M.H. Lim, Metal-associated amyloid-b species in Alzheimer's disease, Curr. Opin. Chem. Biol. 16 (1–2) (2012) 67–73, https://doi.org/10.1016/j.cbpa.2012.01.016.
[19] D.S. Cukierman, A.B. Pinheiro, S.L.P. Castiñeiras-Filho, A.P. Silva, M.C. Miotto, A.D. Falco, A moderate metal-binding hydrazone meets the criteria for a bioinorganic approach towards Parkinson's disease: therapeutic potential, blood-brain barrier crossing evaluation and preliminary toxicological studies, J. Inorg. Biochem. 170 (2017) 160–168, https://doi.org/10.1016/j.jinorgbio.2017.02.020.
[20] M. Ramesh, G. Venkatachalam, Half-sandwich (η6-p-cymene) ruthenium(II) complexes bearing 5-amino-1-methyl-3-phenylpyrazole Schiff base ligands: synthesis, structure and catalytic transfer hydrogenation of ketones, J. Org. Chem. 880 (2019) 47–55, https://doi.org/10.1016/j.jorganchem.2018.10.029.
[21] X.F. Shang, J. Li, K.R. Guo, T.Y. Ti, T.Y. Wang, J.L. Zhang, Development and cytotoxicity of Schiff base derivative as a fluorescence probe for the detection of L-Arginine, J. Mol. Struct. 1134 (2017) 369–373, https://doi.org/10.1016/j.molstruc.2016.12.105.
[22] E.B. Cai, L.M. Yang, C.X. Jia, W.Y. Zhang, Y. Zhao, W. Li, X.Z. Song, M.L. Zheng, The synthesis and evaluation of arctigenin amino acid ester derivatives, Chem. Pharm. Bull. 64 (10) (2016) 1466–1473, https://doi.org/10.1248/cpb.c16-0429.
[23] S. Yu, Y. Gao, X. Mei, T.C. Ren, S. Liang, Z.W. Mao, C.Y. Gao, Preparation of Arg-Glu-Asp-Val peptide density gradient on hyaluronic acid-coated poly(#--caprolactone) film and its influence on the selective adhesion and directional migration of endothelial cells, ACS Appl. Mater. Interfaces 8 (43) (2016) 29280–29288, https://doi.org/10.1021/acsami.6b09375.
[24] E. Weerapana, C. Wang, G.M. Simon, F. Richter, S. Khare, B.D. Myles, M.B.D. Dillon, D.A. Bachovchin, K. Mowen, D. Baker, B.F. Cravatt, Quantitative reactivity profiling predicts functional cysteines in proteomes, Nature 468 (7325) (2010) 790–795, https://doi.org/10.1038/nature09472.
[25] V. Staudacher, V. Djuika, C.F. Koduka, Plasmodium falciparum antioxidant protein reveals a novel mechanism for balancing turnover and inactivation of peroxiredoxins, J. Free Radic. Biol. Med. 85 (2015) 228–236, https://doi.org/10.1016/j.freeradbiomed.2015.04.030.
[26] K.M. Mustaque, A. Subramani, T.K. Shabeer, Amino acid catalyzed synthesis of 2,3-dihydroquinazolin-4(1H)-One derivatives, Lett. Org. Chem. 15 (4) (2018) 246–250, https://doi.org/10.2174/1570178614666171130154814.
[27] J. Shaya, M.A. Deschamps, B.Y. Michel, A. Burger, Air-stable Pd catalytic systems for sequential one-pot synthesis of challenging unsymmetrical amino-aromatics, J. Org. Chem. 81 (17) (2016) 7566–7573, https://doi.org/10.1021/acs.joc.6b01248.
[28] V. Singh, S. Wang, E.T. Kool, Genetically encoded multispectral labeling of proteins with polyfluorophores on a DNA backbone, J. Am. Chem. Soc. 135 (16) (2013) 6184–6191, https://doi.org/10.1021/ja4004393.
[29] X. Chen, A. Tong, Halogenated salicylaldehyde azines: the heavy atom effect on aggregation-induced emission enhancement properties, J. Lumin. 145 (1) (2014) 737–740, https://doi.org/10.1016/j.jlumin.2013.08.051.
[30] D.M. Marin, S. Payerpaj, G.S. Collier, A.L. Ortiz, G. Singh, M. Jones, M.G. Walter, Efficient intersystem crossing using singly halogenated carbomethoxyphenyl porphyrins measured using delayed fluorescence, chemical quenching, and singlet oxygen emission, Phys. Chem. Chem. Phys. 17 (43) (2015) 29090–29096, https://doi.org/10.1039/C5CP04359J.
[31] D.K. Singha, S. Bhattacharya, P. Majee, S.K. Mondal, M. Kumar, P. Mahata, Optical detection of submicromolar levels of nitro explosives by a submicron sized metal–organic phosphor material, J. Mater. Chem. A. 2 (48) (2014) 20908–20915, https://doi.org/10.1039/c4ta05014b.
[32] J. Burgués, J.M. Jiménez-Soto, S. Marco, Estimation of the limit of detection in semiconductor gas sensors through linearized calibration models, Anal Chia Acta 1013 (2018) 13–25, https://doi.org/10.1016/j.aca.2018.01.062.
[33] J. Li, N. Wang, W.T. Liu, H.L. Ding, Y. An, C.W. Lu, A revisit to the Gattermann reaction: interesting synthesis of nitrogen heterocyclic aromatic halides and their fluorescence properties. New J. Chem., 41(20), 12225–12230. https://doi:10.1039/c7nj02672b.
[34] R. Purkait, A. Dey, S. Dey, P.P. Ray, C. Sinha, Designing of Coumarinyl-Picolinoyl hydrazide Schiff base for the fluorescence turn-on-off sequential sensing of Al3+ and nitroaromatics, and electronic device fabrication. New J. Chem. https://doi:10.1039/c9nj03377g.
[35] S. Dey, A. Maity, M. Shyamal, D. Das, S. Maity, D. Debasish, S. Maity, P.K. Giri, N. Mudi, S.S. Samanta, P. Hazra and A. Misra, Antipyrine based fluorescence "turn-on" dual sensor for Zn^{2+} and Al^{3+} and its' selective "turn-off" fluorescence sensing towards 2,4,6-trinitrophenol (TNP) in aggregated state. Photochem. Photobiol. Sci.. https://.doi:10.1039/c9pp00226j.
[36] N. Venkatesan, V. Singh, P. Rajakumar, A.K. Mishra, Isobenzotriazolophanes: a new class of fluorescent cyclophanes as sensors for aromatic nitro explosives - picric acid. RSC Adv., 4(96), 53484-53489. https://doi:10.1039/c4ra06320a.